Simulation of neutrophil deformation and transport in capillaries using Newtonian and viscoelastic drop models

Chunfeng Zhou[1], Pengtao Yue[1,2] and James J. Feng[1,2] *

[1]Department of Chemical and Biological Engineering
University of British Columbia, Vancouver, BC V6T 1Z3, Canada

[2]Department of Mathematics
University of British Columbia, Vancouver, BC V6T 1Z2, Canada

Abstract - It is well known that neutrophils take much longer to traverse the pulmonary capillary bed than erythrocytes, and this is likely due to differences in the structure and rheology of the cells. In this study, we simulate the transit of a neutrophil in a capillary using a Newtonian drop model and a viscoelastic drop model. The cell membrane is represented by an interface with isotropic and constant tension, and the cell motion and deformation are described by a phase-field method. The governing equations are solved using finite elements in an axisymmetric geometry, and the thin interfaces are resolved by mesh adaptivity. With a fixed pressure drop, the entry of a cell into a capillary consists of several stages in which the flow rate varies in distinct manners. The entrance time is consistent with experimental measurements. It decreases with the pressure drop, increases with the cell viscosity and generally decreases with the relaxation time of a viscoelastic cytoplasm. The capillary geometry has a strong effect on the entry and transit of a neutrophil. The entrance time increases sharply when the capillary diameter decreases or when the capillary is constricted by a pinch.

Key Terms: entrance time, cytoplasmic rheology, viscoelasticity, numerical simulation, phase-field method.

---

*Corresponding author. E-mail: jfeng@CHML.UBC.CA

I. INTRODUCTION

Neutrophils often encounter narrow capillary segments during their transit through the pulmonary and systemic microcirculations. Because the neutrophil diameter (6–8 μm) often exceeds the diameter of a pulmonary capillary (2–15 μm),[1,2] cell deformation is necessary for passage. It is well known that neutrophils take much longer to traverse the pulmonary capillary bed than erythrocytes.[3] As a result, white cells accumulate in the lungs and form a reservoir from which they may be readily recruited when needed.[1,4] As the pulmonary bed consists of 50–100 capillary segments,[5,6] the longer transit time for neutrophils likely reflects their relatively poor deformability,[7,8] which in turn depends on the structure and mechanical properties of the cell: membrane rigidity, cytoplasmic viscosity and viscoelasticity, and the properties of the nucleus.

Measuring leukocyte deformation and transit in vivo is a difficult task,[3] and so far our understanding of the mechanical behavior of leukocytes has come mostly from micropipette aspirations in vitro. By measuring the time-dependent cell deformation at a controlled pressure, cell viscosity, cortical tension and elastic modulus can be estimated by treating the cell as a homogeneous continuum.[9,10] As a sort of rheometry, aspiration experiments yield fundamentally important data. But they do not produce direct information on cell transit in capillaries. The Cell Transit Analyzer[11] combines the aspiration process with subsequent passage through cylindrical pores, and allows rapid measurements of transit time. However, the cell entry and departure from the micropore is monitored from the attendant pulses in electric conductivity across the filter. The actual deformation of the cell is unknown and the interpretation of the signal is subject to much uncertainty.[11,12]

Recently, Yap and Kamm[2] carried out an experiment using microfluidic channels that seems to have overcome previous difficulties. The device allows direct observation of neutrophil deformation and activation upon entering a microfluidic channel, as well as measurement of the cell entrance time as a function of the pressure drop imposed across the microfluidic channel. The present work is motivated by Yap and Kamm's experiment, and aims to extract a fundamental understanding of the cell entry process using dynamic simulations. Yap and Kamm[2] also reported interesting results on neutrophil activation probed by microrheology and pseudopod formation. These will not be accounted for in our simulations.

Analyzing the physical and mechanical processes on the single-cell level remains a challenge, especially when taking the living and dynamic nature of the cell into consideration.[13] Lim *et al.*[14] reviewed the quantitative mechanical models developed so far for the cell. Generally, these adopt either a microstructural approach or a continuum approach. The former is based on the cytoskeleton as the main structural component, and has been used widely to investigate cytoskeletal mechanics in adherent cells.[15] On the other hand, the continuum approach takes the cell as comprising homogeneous materials with certain effective properties. Although providing less insight into the details of intra-cellular processes, the latter is simpler and has found applications in simulating large-scale transient behavior of suspended cells such as the corpuscles in the blood.[16–18]

Continuum cell models come in several flavors. The Newtonian liquid drop model[9,19] sees the cell as a homogeneous Newtonian drop enclosed by a cortex that has a constant and isotropic tension and negligible viscous dissipation. Non-Newtonian drop models, such as the shear-thinning model[20] and the viscoelastic Maxwell model,[21] have since been developed to reflect the non-Newtonian rheology of the cytoplasm in leukocytes. Furthermore, compound drop models[22–25] explicitly account for the cell nucleus as a drop suspended in the cytoplasm. The cell and nuclear membranes are taken to be interfacial layers with differing interfacial tensions. So far, micropipette aspiration has been the benchmark problem for testing these models, and the prediction has been remarkably good considering the simplicity of the models.[19,21,26,27] Moreover, the models have been used to simulate other modes of controlled deformation in relatively simple geometries, e.g., recovery in a quiescent medium[25,28,29] and deformation in elongational flows[24] and shear flows.[18,30] Most recently, the compound drop models have been applied in simulating the adhesion of leukocytes on the endothelium.[31–33] However, only a few simulations have been carried out on the transit of suspended neutrophils, either through a single capillary[6,34] or an idealized capillary network.[5]

The present study consists of dynamic simulations, based on the Newtonian and viscoelastic drop models, of the deformation and transit of neutrophils through capillaries that roughly correspond to the experiments of Yap and Kamm.[2] Specifically, we study the entry of a neutrophil from a larger vessel into a narrow capillary using geometry and parameter values based on the Yap-Kamm experiments. The entrance time, the cell deformation and

the subsequent motion within the capillary will be compared with observations. The focus of the study will be on how cytoplasmic rheology affects the entry of a neutrophil into a thin capillary. The nucleus is not explicitly accounted for, and the cytoplasmic rheology should be understood as an averaged property of the complex mixture of the nucleus, cytosol and suspended organelles. Furthermore, we have neglected two physiologically important factors. First, the cell membrane is treated as thin interfaces having a constant cortical tension, with no elastic resistance against bending and in-plane shearing and no viscous dissipation. We recognize that membrane elasticity has an important role in cell deformation that has received a great deal of research.[17,35] Although membrane elasticity may be incorporated into the phase-field theory,[36,37] we defer the implementation to a future effort. Second, we have not accounted for the glycocalyx on the inner walls of the capillary, which is known to greatly increase resistance on red blood cells.[38,39] This is partly because very little is known of the glycocalyx on the pulmonary endothelium, and partly because incorporating the porous layer model would greatly increase the complexity of the flow simulation. So far, the only multi-dimensional computation that accounts for the glycocalyx used a drastically simplified model of a frictionless contact surface.[6]

In the context of computational fluid dynamics, our problem is a complex one because of the moving and deforming interfaces and the non-Newtonian rheology of the fluid components, each being a major computational challenge.[40,41] Recently, we have developed a diffuse-interface method that incorporates the moving interface and non-Newtonian rheology in a unified variational framework.[42,43] Implemented using spectral methods and finite elements, the method has been applied successfully to several problems in drop dynamics of complex fluids,[44–50] and will be adapted here to the task of neutrophil deformation and transport.

II. THEORY AND NUMERICAL METHODS

Our diffuse-interface model was developed mainly for simulating interfacial dynamics in complex fluids. For any binary blend, the two nominally immiscible components are assumed to mix in a narrow interfacial layer and store a mixing energy. Across the interfacial layer, physical properties such as viscosity and density change steeply but continuously. The interfacial position and thickness are determined by a phase-field variable ϕ whose

evolution is governed by a Cahn-Hilliard equation. The interfacial tension is given by the mixing energy. This way, the structure of the interface is rooted in molecular forces and calculated from a convection-diffusion equation; there is no longer a need for tracking the interface. Moreover, the model uses an energy-based formulation that incorporates the non-Newtonian rheology of microstructured fluids with ease. This is the main reason for our selecting this methodology. A more in-depth discussion of the advantages and disadvantages of the diffuse-interface model, vis-à-vis the classical sharp-interface model and other interface regularization methods, can be found in the literature.[42,43,51]

The above methodology has been implemented in a finite-element package AMPHI (Adaptive Meshing with phase field ϕ). Yue *et al.*[48] have described the code in detail and presented numerical experiments to establish its validity and accuracy. In this paper, we will only summarize the main ideas and give the governing equations. To be specific, consider a Newtonian fluid in contact with a viscoelastic Oldroyd-B fluid, the interface between the two being diffuse with a small but non-zero thickness. We define a phase-field variable ϕ such that the concentrations of the non-Newtonian and Newtonian components are $(1 + \phi)/2$ and $(1 - \phi)/2$, respectively. Then ϕ takes on a value of 1 or -1 in the two bulk phases, and the interface is simply the level set $\phi = 0$. Starting with the system's free energy, comprising the mixing energy of the interface and the bulk elastic energy in the Oldroyd-B fluid, we can derive the following set of governing equations:[44,48]

$$\frac{\partial \phi}{\partial t} + \boldsymbol{v} \cdot \nabla \phi = \gamma \nabla^2 G, \tag{1}$$

$$G = \lambda \left[-\nabla^2 \phi + \frac{\phi(\phi^2 - 1)}{\epsilon^2} \right], \tag{2}$$

$$\boldsymbol{\tau}_p + \lambda_H \boldsymbol{\tau}_{p(1)} = \mu_p [\nabla \boldsymbol{v} + (\nabla \boldsymbol{v})^T], \tag{3}$$

$$\boldsymbol{\tau} = (\frac{1 - \phi}{2} \mu_n + \frac{1 + \phi}{2} \mu_s)[\nabla \boldsymbol{v} + (\nabla \boldsymbol{v})^T] + \frac{1 + \phi}{2} \boldsymbol{\tau}_p, \tag{4}$$

$$\rho \left(\frac{\partial \boldsymbol{v}}{\partial t} + \boldsymbol{v} \cdot \nabla \boldsymbol{v} \right) = \nabla \cdot (-p\boldsymbol{I} + \boldsymbol{\tau}) + G\nabla \phi + \rho \boldsymbol{g}, \tag{5}$$

$$\nabla \cdot \boldsymbol{v} = 0, \tag{6}$$

where G is the chemical potential and γ is the mobility parameter; λ and ϵ are the interfacial energy density and capillary width, respectively. The polymer stress $\boldsymbol{\tau}_p$ obeys the Maxwell equation, with the subscript $_{(1)}$ denoting the upper convected derivative and λ_H being the polymer relaxation time.[52] μ_p and μ_s are the polymer and solvent contributions to the

shear viscosity of the Oldroyd-B fluid, and μ_n is the viscosity of the Newtonian phase. ρ is a mixture density: $\rho = \frac{1+\phi}{2}\rho_1 + \frac{1-\phi}{2}\rho_2$, ρ_1 and ρ_2 being the densities of the Oldroyd-B and Newtonian components, and $\boldsymbol{g}$ is the gravitational acceleration. As demonstrated elsewhere,[44,48] the diffuse interface has two important features: (*a*) The interface has a thickness on the order of 5ϵ. The Cahn-Hilliard dynamics ensures that it neither collapses into a sharp surface nor diffuses into a wide region. (*b*) In the limit of $\epsilon \to 0$, the above system reduces to the familiar sharp interface formulation, and $2\sqrt{2}\lambda/3\epsilon$ gives the interfacial tension.[42] The velocity and shear stress are continuous across the interface and the normal stress has a jump consistent with the interfacial tension. To accurately reproduce the cortical tension on a thin "membrane", therefore, we must use an ϵ that is much smaller than the overall dimension and must resolve the ϕ profile adequately within the thin interface. This is why adaptive meshing is essential to AMPHI.[48]

These equations are discretized on a finite-element grid using the Petrov-Galerkin formulation with streamline upwinding for the constitutive equation. We will concern ourselves only with axisymmetric geometry in this study, and the 2D computational domain is covered by an unstructured grid of triangular elements. To resolve the thin interfacial region, we have used an adaptive meshing scheme based on the public-domain package GRUMMP.[53] The scheme allows one to control the spatial gradient of grid size using a scalar field. In our application, the phase-field variable ϕ is a natural choice for this function. Thus, we have a belt of refined triangles covering the interfacial region. As the interface approaches the edge of the belt, remeshing is performed with the mesh upstream of the interface being refined by edge bisection and/or node insertion while that left behind being coarsened. Typically the interfacial layer requires roughly 10 grid points to resolve, and remeshing happens over tens of time steps. We use implicit time-stepping, with Newton iteration at every step to handle the nonlinearity in the equations. The time step is automatically adjusted according to a set of criteria based on the normal velocity of the interface and the bulk velocity. Numerical experiments with grid refinement and time-step refinement have been carried out,[48] and adequate resolution is ensured for the simulations presented in the following.

III. SIMULATIONS USING THE NEWTONIAN DROP MODEL

As the simplest model for a neutrophil, we have a liquid drop containing a homogeneous viscous Newtonian fluid that represents the cytoplasm and nucleus in an average sense. The
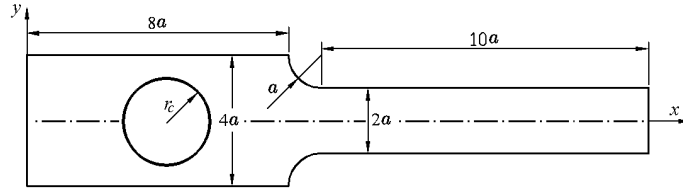
Figure 1: The geometric setup for simulating a neutrophil's entrance into a capillary. Two cylindrical tubes are connected by an arc of 90°. Shown is the meridian plane and the upper half is the computational domain.

interfacial tension σ represents a constant and isotropic tension in the cell membrane. The drop fluid, or "cytoplasm", has a density ρ_c and a viscosity μ_c, and the cell is suspended in a matrix of density ρ_m and viscosity μ_m. Before deformation, the spherical cell has a radius r_c. To simulate the entry of the neutrophil into a capillary, we use the axisymmetric computational domain illustrated in Fig. 1. The narrow capillary downstream of the contraction has a radius a and length $L = 10a$. A constant pressure drop ΔP is applied over the entire length of the domain $19a$. To construct the dimensionless groups controlling the process, we use a as the characteristic length and $V_f = \Delta P a^2 / (8\mu_m L)$ as the characteristic velocity. Note that V_f is the average velocity in a Poiseuille flow through a uniform pipe of radius a with pressure gradient $\Delta P / L$. Then five dimensionless groups can be constructed:

$$Ca = \frac{\mu_m V_f}{\sigma}, \tag{7}$$

$$Re = \frac{\rho_m V_f a}{\mu_m}, \tag{8}$$

$$\alpha = \frac{\rho_c}{\rho_m}, \tag{9}$$

$$\beta = \frac{\mu_c}{\mu_m}, \tag{10}$$

$$\zeta = \frac{r_c}{a}, \tag{11}$$

where the capillary number Ca indicates the ratio between viscous and capillary forces, and the Reynolds number Re represents the ratio between inertial and viscous forces. The characteristic flow time is $t_f = a/V_f$, and the flow rate will be scaled by $Q_f = \pi a^2 V_f$. For brevity, we use the same symbols for dimensional and dimensionless variables, but will explicitly indicate which is meant where confusion may arise.
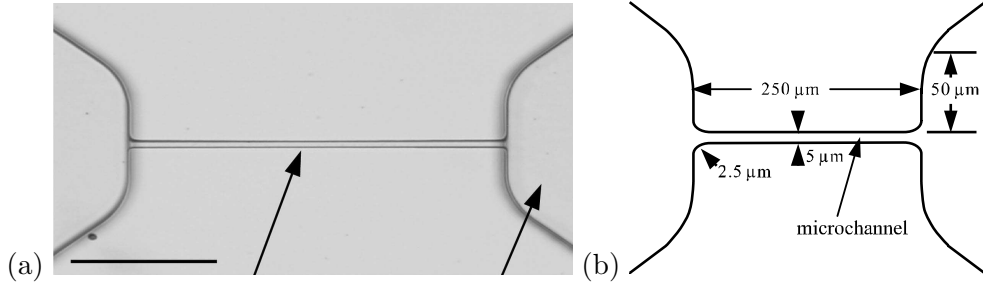
Figure 2: (a) The microchannel of Yap and Kamm.[2] The scale bar is 100 μm, and the two arrows indicate the microchannel and the reservoir. (b) Schematic showing the dimensions of the microchannel. Its cross-section is rectangular with a width of 5 μm and a depth of 2.5 μm. After Yap and Kamm;[2] ©2005 the American Physiological Society.

The cell radius, effective viscosity and cortical tension of the neutrophil are taken from the literature:[2,9,14] $r_c = 3.5$ μm, $\mu_c = 2.2$ poise and $\sigma = 0.035$ dyn/cm. The plasma density and viscosity are essentially those of water. The neutrophil is nearly neutrally buoyant and we have taken the density ratio α to be unity in all the simulations. The dimensions in Fig. 1, with $a = 2$ to 2.5 μm, approximate these in the experiment of Yap and Kamm[2] (Fig. 2). But their microchannel has a rectangular cross-section and an exact match is impossible. For the typical flow rates in the experiments,[2] the capillary number Ca ranges up to 0.1 and the Reynolds number $Re = O(10^{-3})$. Thus inertia has little part in the dynamics to be discussed. The viscosity ratio β is on the order of 200 for an activated neutrophil and may be as large as 10^4 before activation.[2,9,14] Highly viscous cells deform less and tend to press tightly against the channel walls at the entrance. For lack of a proper treatment of the membrane-wall interaction, such cells often stick to the wall. This drawback limits us to β values on the order of 50. For convenience, therefore, we have used relatively small β values. Varying β between 1 and 16 shows a clear trend in the results and we did not explore higher β values systematically.

As mentioned before, we use an adaptive meshing scheme to resolve the thin interfacial region so as to produce an accurate cortical tension. In all the simulations, we have used a capillary width $\epsilon = 0.008a$. The finest grids occur at the interface with grid size $h_1 = 0.005a$, while the bulk mesh size inside and outside the cell are $h_2 = 0.12a$ and $h_3 = 0.2a$, respectively. These, along with the time step Δt, have been tested in numerical experiments[48] to ensure adequate resolution. At the beginning of the simulation, the cell is

placed on the centerline at $x = 5a$ and the velocity is zero everywhere. Then the pressure drop ΔP, imposed over the whole length of the domain, drives a flow from the left to the right in Fig. 1. At the inlet and the outlet, we set the boundary conditions to be $v = 0$ and $\partial u/\partial x = 0$. On the centerline we use symmetry conditions: $v = 0$ and $\partial u/\partial y = 0$.

A. The process of cell deformation and entrance

For one set of parameters, the process of cell entrance is illustrated by the snapshots in Fig. 3. The variations of the flow rate Q and cell length l are plotted in Fig. 4 as functions of time. One may discern four stages in the process. (i) First, the neutrophil deforms and moves into the contraction while the flow rate drops sharply ($t < 5$). This is because the front of the cell is sucked into the capillary and plugs most of the flow area. The cell length increases steadily, and this stage continues until roughly half of the cell is within the capillary. (ii) Once the plugging of the capillary has reached its maximum level, the flow rate more or less keeps constant until the whole cell enters the capillary ($5 < t < 9$). The elongation of the cell continues in this second stage; its rear is "held" by the contraction while its front is stretched by the flow (Fig. 3c). (iii) The third stage is a transient as the rear of the cell clears the contraction ($9 < t < 12$). As the contraction loses its "grip" on the cell (Fig. 3d), the high capillary pressure inside its rear produces a sudden forward flow and a retraction of the cell's back surface. This temporary shortening of the cell (see Fig. 4) in turn increases the blockage in the capillary and causes the flow rate to drop. Both l and Q recover in time as the cell attains an equilibrium shape. (iv) Finally, the cell moves downstream with a constant shape and velocity ($t > 12$).

The scenario described above is observed for most of the simulations but is *not universal*; some aspects vary depending on the parameter values. In section III.C, we will see different behaviors of the flow rate in stage (ii) for higher and lower cell viscosities (cf. Fig. 7). In the more extreme case of very high pressure drops, both the flow rate and the cell length vary monotonically, and no obvious stages can be discerned. This is because the cell is highly elongated by the contraction flow upstream of the capillary and the entry becomes relatively uneventful. We have observed in the simulations that the flow rate Q and cell length l generally vary in opposite directions (cf. Fig. 4). This will be explained in the next subsection in terms of the increased flow resistance due to the cell.
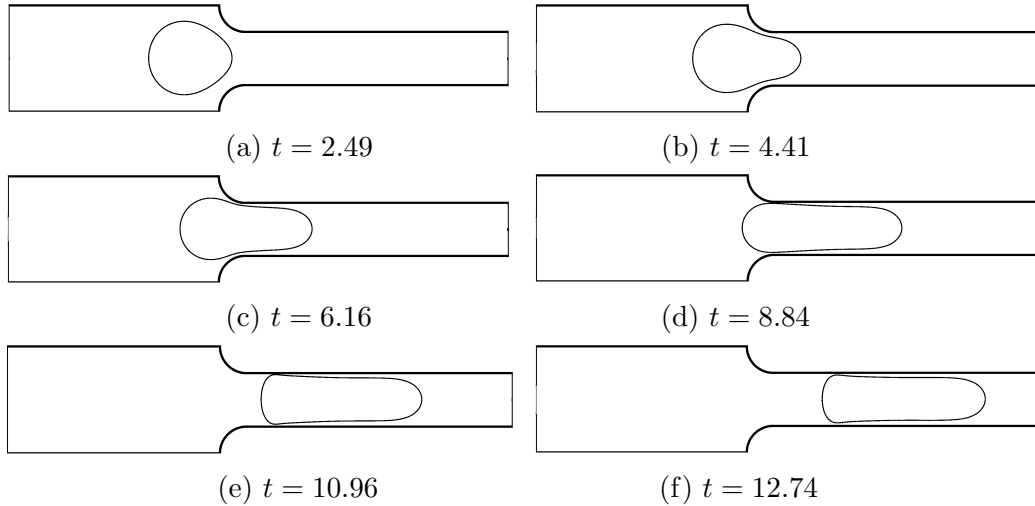
(a) $t = 2.49$ (b) $t = 4.41$

(c) $t = 6.16$ (d) $t = 8.84$

(e) $t = 10.96$ (f) $t = 12.74$

Figure 3: Snapshots of the neutrophil during its entrance into the capillary. $Ca = 0.0893$, $\beta = 3$ and $\zeta = 1.4$. Time is made dimensionless by $t_f = a/V_f$.
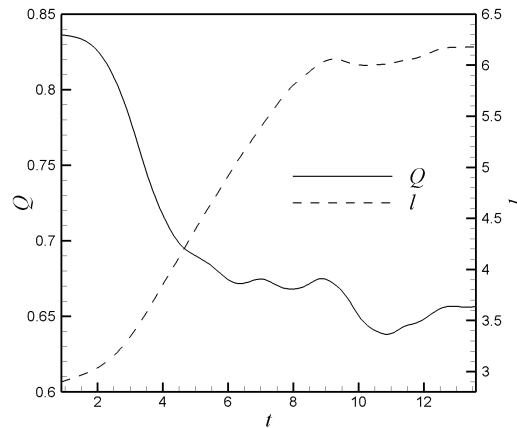

Figure 4: Variations of the flow rate Q and cell length l during the entrance process. Q is made dimensionless by Q_f. The cell length l is the distance between the foremost and rearmost points of the cell and is scaled by a. $Ca = 0.0893$, $\beta = 3$ and $\zeta = 1.4$.

B. The entrance time

As in Yap and Kamm's experiment,[2] we define the entrance time τ_{ent} as the time interval between the leading edge of the cell crossing the entry to the capillary (namely, the axial position where the straight portion of the capillary starts) and its trailing edge clearing the entry. Figure 5 shows the numerically computed τ_{ent} for a range of applied pressure drop (or capillary number). The dimensionless entrance time increases with the imposed
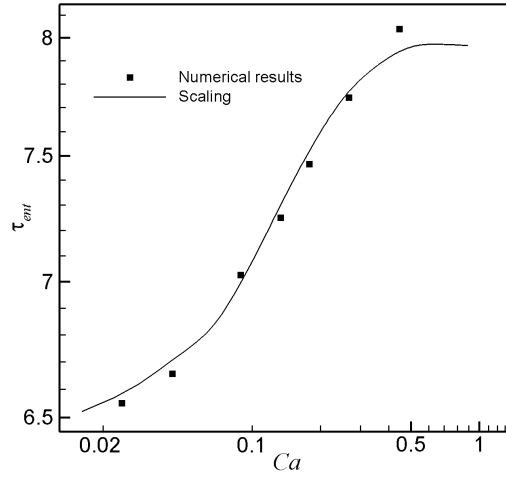
10

Figure 5: Log-log plot of the dimensionless entrance time τ_{ent} as a function of the capillary number Ca. The data points are numerical results while the solid curve represents Eq. (18) derived from scaling arguments. $\beta = 3$ and $\zeta = 1.4$. Time is made dimensionless by a/V_f, and Ca is defined using the applied pressure ΔP in Eq. (7).

pressure; the slope suggests a weak power-law with an index of around 0.1. Intuitively, the *dimensional* τ_{ent} should decrease with ΔP or the velocity V_f since a higher pressure will induce a faster flow and a more rapid entry of the cell. If the cell followed the surrounding fluid perfectly, its velocity would be proportional to V_f and the *dimensionless* entrance time, scaled by a/V_f, would be independent of the imposed pressure or the flow rate. In reality, however, the cell's motion is hindered by the channel walls. The weak increase of τ_{ent} with Ca in Fig. 5 suggests that the cell lags the matrix fluid more at faster flow rates. In the following, we will provide a more quantitative explanation for the effect using scaling arguments.

With negligible inertia, the constant pressure drop ΔP is entirely expended on overcoming the viscous friction on the channel walls. The presence of the cell increases the wall friction in its vicinity. To quantitate this effect, we adopt a simplified geometry of the cell. Figure 3 suggests that during much of the entry process, the rear of the cell is constricted by the pinch and hardly moves forward. The front of the cell extends into the capillary in a slug shape. We make three assumptions about the gap δ between the cell and the capillary wall: (*a*) δ is much smaller than the capillary radius a; (*b*) δ is constant along the length of the cell l_c that is inside the capillary; (*c*) δ does not change in time during the entry

11

process. Volume conservation of the cell then allows us to calculate δ from the cell length l_e at the end of the entry process:

$$\delta = a - \sqrt{\frac{4r_c^3}{3l_e}}, \tag{12}$$

r_c being the radius of the initial spherical cell. Note that we have assumed a cylindrical shape for the part of the cell inside the capillary. Now the pressure drop ΔP can be divided into two parts: ΔP_{cell} to overcome the elevated wall friction over the cell length l_c inside the capillary, and ΔP_{wall} for the rest of the channel wall. The former will be calculated from the shear rate inside the gap δ, while the latter is to be estimated from the pressure drop needed to drive the same flow rate in the absence of the cell. This dichotomy is not exact, and further simplifications will be made in the following. The errors will be lumped in the end into a single adjustable coefficient.

At the instantaneous flow rate Q, the velocity within the gap scales with $Q/(2\pi a\delta)$ and the viscous shear stress scales with $\mu_m Q/(2\pi a\delta^2)$. Because of the tangential velocity on the cell surface, the actual flow rate through the gap δ is smaller than Q. But this discrepancy will be accounted for by the adjustable coefficient. Balancing ΔP_{cell} against the shear stress in the gap leads to the scaling

$$\Delta P_{cell} \propto \frac{\mu_m}{\pi a^2 \delta^2} Q l_c. \tag{13}$$

For ΔP_{wall}, we modify the Poiseuille formula on account of the wider section and the contraction upstream of the capillary:

$$\Delta P_{wall} = \frac{9.9\mu_m}{\pi a^4} Q(L - l_c), \tag{14}$$

where the coefficient 9.9 is determined for our geometry from pressure drop in the absence of the cell. Now we may write the total pressure drop as

$$\Delta P = \Delta P_{wall} + \Delta P_{cell} = \frac{9.9\mu_m}{\pi a^4} Q(L - l_c) + c\frac{\mu_m}{\pi a^2 \delta^2} Q l_c. \tag{15}$$

The adjustable parameter c accounts for the geometric simplifications made above and the slip velocity on the cell surface. Therefore, it should depend on the geometry and the cell-matrix viscosity ratio β. It is to be determined by fitting the entrance time. As the presence of the cell increases the local wall friction, Eq. (15) implies that if l_c increases, the flow rate Q will decrease and vice versa. This explains the trend in Fig. 4.

12

As $l_c(t)$ is the cell length within the capillary, it increases in time from 0 at the start of cell try to l_e at the end. Thus, the entry time τ_{ent} is largely determined by how fast the cell is elongated by the flow. Since the rear of the cell moves little in this process (cf. Fig. 3), cell elongation depends on the motion of its leading edge. We assume that this motion is at the instantaneous average velocity within the capillary: $dl_c/dt = Q/(\pi a^2)$. Then Eq. (15) leads to an ordinary differential equation for the cell length $l_c(t)$:

$$\Delta P = \mu_m \left[\frac{9.9(L - l_c)}{a^2} + \frac{cl_c}{\delta^2} \right] \cdot \frac{dl_c}{dt}. \tag{16}$$

Now the entrance time τ_{ent} can be obtained by integrating the above equation:

$$\tau_{ent} = \frac{\mu_m}{\Delta P} \left[\frac{4.95(2Ll_e - l_e^2)}{a^2} + \frac{cl_e^2}{2\delta^2} \right]. \tag{17}$$

Noting that $L = 10a$ and scaling τ_{ent} by t_f and the lengths by a, we arrive at the dimensionless entrance time

$$\tau_{ent} = \frac{1}{80} \left(99l_e - 4.95l_e^2 + \frac{cl_e^2}{2\delta^2} \right). \tag{18}$$

The cell length l_e depends on ΔP or Ca. Figure 6 indicates that the cell is longer (and thinner) inside the capillary at higher capillary number. This dependence cannot be easily modeled, however. Generally speaking, $l_e(Ca)$ is determined by the balance between capillary and viscous forces. But it is also influenced by the wall confinement and the inner circulation. Thus, we have decided to use the numerical results Fig. 6 in Eq. (18). Finally the coefficient c can be determined by a least-square fitting of the equation to numerical data in Fig. 5. The best fitting is achieved for $c = 0.13$ in this case. The fact that $c < 1$ is mainly because the flow rate through the gap δ is typically only a fraction of Q on account of the cell's motion.

Equation (18) describes the numerical results well at low Ca, but underestimates τ_{ent} at high Ca. As the pressure drop ΔP and Ca increase, the cell becomes thinner and more elongated. Not only does this violate the assumption $\delta \ll a$, but the cell develops a conic nose and the uniform gap assumption becomes less accurate. Hence the failure of the scaling at higher Ca. Finally, the scaling argument indicates that the weak increase of τ_{ent} with Ca in Fig. 5 is due to the weak rise of the cell length l_e with Ca in Fig. 6. Since the latter is plotted in dimensionless parameters, it can be interpreted alternatively as the cell length
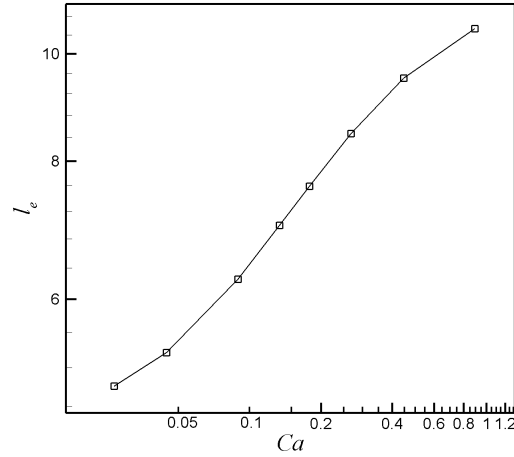
13

Figure 6: The cell length l_e at the end of the entry process as a function of the capillary number Ca for $\zeta = 1.4$ and $\beta = 3$.

l_e decreasing with the interfacial tension σ, which is intuitively obvious. Thus, the entrance time τ_{ent} is expected to decrease with the cortical tension σ at a constant pressure drop.

C. Effect of cytoplasmic viscosity

In the above simulations, the viscosity ratio between the fluid inside the cell and the suspending medium is set to be $\beta = 3$. This is much below the cytoplasm-plasma viscosity ratio in vivo,[2,9] as well as the experimental value in Yap and Kamm[2] who used water as the suspending fluid. As indicated earlier, the use of a modest β value is a numerical expedient. In this subsection, we will vary the viscosity ratio to see how the cytoplasmic viscosity affects the process of neutrophil entry and passage in a capillary.

We carried out a series of numerical simulations at capillary numbers $Ca = 0.0893$. The viscosity ratio β is varied between 1/16 to 16 with all other dimensionless groups unchanged. At higher Ca, we were able to reach larger β values without having the cell stuck on the walls, but the results have the same trend as discussed below. For three β values, Fig. 7 illustrates the temporal evolutions of the flow rate Q and total cell length l. In all three cases, the flow rate manifests the stages described in Section III.A. However, the character of the *second stage* changes with β. For a small β, Q keeps constant or even increases in this stage, whereas for a large β, Q continues to decrease, albeit at a milder slope than in the previous stage. Recall that at the second stage, the cell has reached maximum blockage
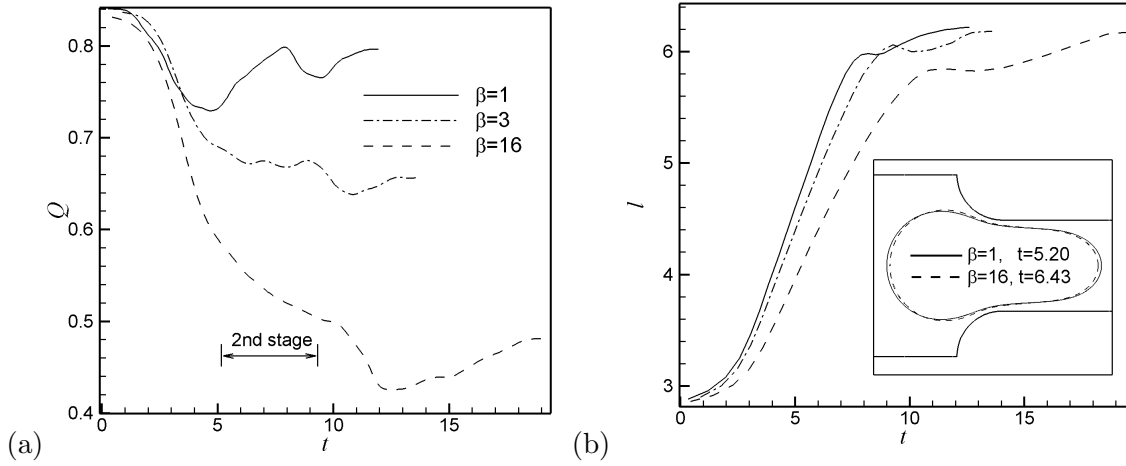
14

Figure 7: The flow rate (a) and cell length (b) during cell entry for three viscosity ratios. $Ca = 0.0893$, $\zeta = 1.4$. Q, t and l have been made dimensionless by $\pi a^2 V_f$, a/V_f and a. The inset in (b) compares the blockage of the entrance for two β values.

of the capillary, with roughly half of the cell inside the capillary (cf. Fig. 4). The differing trends in Q are because the cell approaches the capillary entrance with differing shapes and thus causes differing degrees of blockage. For a lower cell viscosity and smaller β, the cell deforms more quickly in the contraction flow upstream of the capillary, and has already developed the protruding nose by the time the cell starts to enter the capillary. As the front of the cell extends further into the capillary, the rear deflates simultaneously, thereby enlarging the gap between the cell surface and the wall at the "shoulder" of the contraction where the blockage is the greatest. Thus, Q increases in time in stage two. A more viscous cell, on the other hand, has a stouter shape when it approaches the capillary and thus plugs the entry more severely. The inset in Fig. 7(b) shows a narrower gap at the shoulder for $\beta = 16$ than $\beta = 1$, and this explains the generally lower Q for higher β. Moreover, as the cell continues to deform and its front protrudes into the capillary, the gap between the cell and the wall is squeezed further at the shoulder, causing the continued decline in Q until the cell is completely inside the capillary.

Then it comes as no surprise that the entrance time τ_{ent} increases with β (Fig. 8). The effect is rather weak, and follows a power law with an index of 1/7. Evidently, this is because a more viscous cell deforms more slowly as in Fig. 7(b). In fact, the cell has an inherent visco-capillary time scale $\bar{\mu} r_c / \sigma$, where $\bar{\mu}$ is a certain combination of the cell and
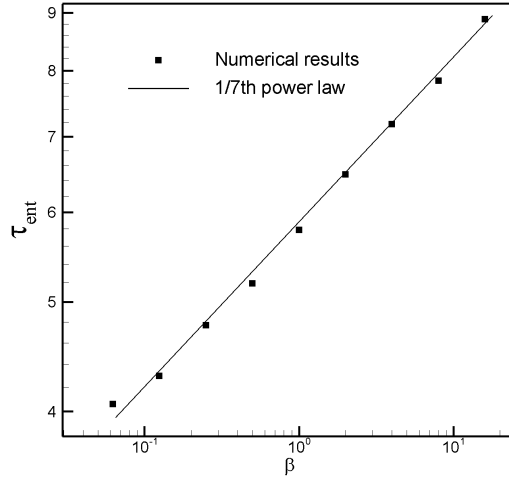
15

Figure 8: The entrance time as a function of the viscosity ratio. The matrix viscosity is kept fixed while the cell viscosity is varied. $\zeta = 1.4$.

matrix viscosities.[50] The fact that τ_{ent} scales with $\beta^{1/7}$ instead of β is because the external fluid, whose viscosity is kept constant, also affects the deformation process.

D. Effects of capillary diameter and geometry

While the human neutrophil has a diameter close to 7 μm, the diameter of the pulmonary capillary ranges from 2 μm to 15 μm.[2] Naturally, a neutrophil will enter and traverse a larger capillary much more readily than a narrower one. In exploring how the entrance time τ_{ent} depends on the capillary diameter a, it is more convenient to use the cell radius r_c as the characteristic length. Then varying a amounts to varying the size ratio $\zeta = r_c/a$ without affecting any of the other dimensionless groups. However, to match the data in prior subsections where $r_c = 1.4a$, we have used $r_c/1.4$ instead of r_c as the characteristic length. Similarly, the characteristic velocity $V_f = \Delta P (r_c/1.4)^2/(8\mu_m L)$ is used in scaling τ_{ent} and Q and in defining the capillary and Reynolds numbers. The radius of the upstream vessel is kept constant at $1.43r_c$.

Not surprisingly, the entrance time increases steeply as the capillary narrows (Fig. 9a). The $\tau_{ent}(\zeta)$ curve does not follow a power-law, its slope on the log-log plot increasing from 3.2 for the smallest ζ to 5 at the upper bound. Bathe *et al.*[6] computed the transit time of a cell in a capillary with a constriction, and correlated the results with the minimum radius
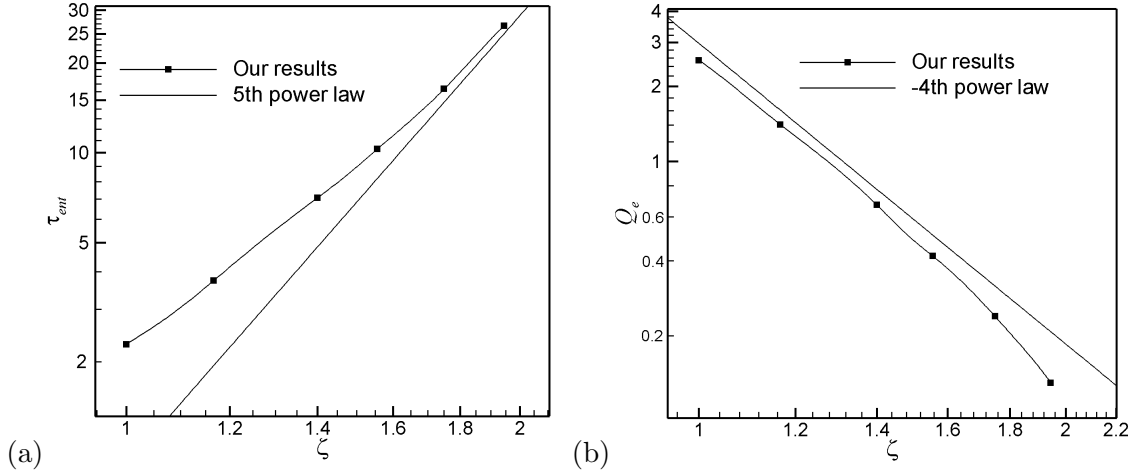
16

Figure 9: Effects of the capillary size on (a) the entrance time τ_{ent} and (b) the flow rate Q_e at the end of the cell entry. $Ca = 0.0893$ and $\beta = 3$.

at the nip of the constriction. If we equate this minimum radius with our capillary radius a, their correlation is $\tau_{ent} = \tau_0(\zeta^5 - 1)$ in our notation. Despite the different geometry, the 5th power law is comparable to our data in Fig. 9(a) for large ζ. As ζ decreases toward unity, Bathe *et al.*'s empirical equation deviates from a 5th power law, as do our data. Since the pre-factor τ_0 cannot be defined unambiguously for our geometry, a more detailed comparison cannot be made.

As an indication of the transit time of the cell once it is entirely inside the capillary, Fig. 9(b) plots the instantaneous flow rate Q_e at the end of the entrance process (when the cell's trailing edge clears the entry) as a function of the capillary radius. Note that Q_e has been scaled by a characteristic value $\pi(r_c/1.4)^4 \Delta P/(8\mu_m L)$ that is independent of a. For the Poiseuille flow in a pipe, the flow rate is expected to scale as a^4 or ζ^{-4}. Over the range of ζ in Fig. 9(b), the data fall on a gentle curve whose slope is close to -4. The deviation from the power law is such that toward the upper bound of ζ (i.e., for the smallest capillaries), Q_e decreases more than ζ^{-4} as the capillary radius decreases. This is because of the impenetrable cell surface hindering the flow in its vicinity. The effect becomes stronger for smaller capillaries which are more severely plugged by the cell.

A related issue is how a neutrophil traverses a *partially blocked* capillary. It has long been known that in falciparum malaria, parasitized erythrocytes tend to adhere and block
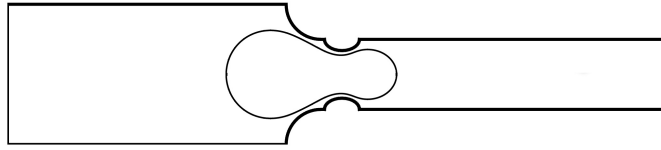
Figure 10: A snapshot of a neutrophil entering the capillary with an elliptic obstacle after the entrance. $Ca = 0.0893$, $\beta = 3$ and $\zeta = 1.4$.

the lumen of brain capillaries,[54] with potentially fatal consequences. More recently, direct visualization in a microfluidic channel demonstrated that P. falciparum-infected erythrocytes lose their elasticity and deformability and become lodged in the channel.[55] Bathe *et al.*'s simulation[6] used a geometry of a cylindrical capillary with a constriction formed by a smooth protrusion on the inner walls. Although this is intended to mimic the entrance to a segment in the pulmonary capillary network, their result suggests that the passage of a neutrophil will be greatly delayed by blockage of a capillary.

Our computational geometry in Fig. 10 is based on images of brain capillaries partially obstructed by sequestered erythrocytes.[54] The blockage is modeled by an annular pinch in the shape of half an ellipse in the meridian plane. The major axis of the ellipse is fixed and equal to the capillary radius a, and its minor axis is varied to change the degree of constriction. We denote the height of the protrusion (or the minor semi-axis of the ellipse) by h. The constriction is right after the entry; the ellipse starts where the circular arc of the contraction would have connected to the wall of the capillary. In the results to be presented, we have reverted to using a as the characteristic length.

Figure 11 shows that the entrance time τ_{ent} increases with h, and the increase becomes steeper when the blockage gets more severe. When the obstacle height is 30% of the capillary radius, τ_{ent} is almost doubled. Conceivably, for a critical h value, the cell will fail to pass completely, and this critical h should increase with the imposed pressure drop or Ca. Figure 11 also plots the aforementioned correlation of Bathe *et al.*[6] recast in terms of h. Since our obstacle is elliptic and theirs is part of a circular arc, the pre-factor τ_0 is determined by taking the average between the major and minor axes of our ellipse as the diameter of the circular arc. The correlation shows a much stronger effect than our results. This is mostly because in their geometry, the obstacle has a radius greater than the cell
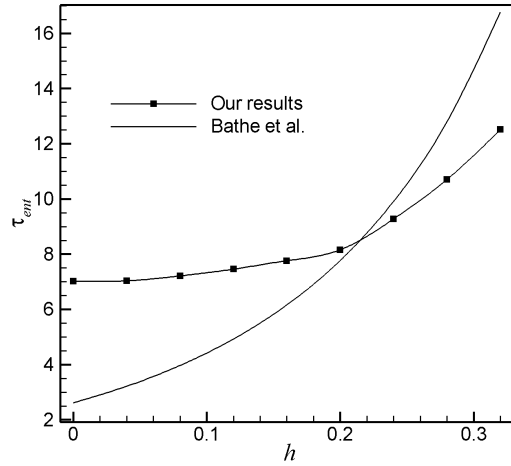
18

Figure 11: The entrance time as a function of the obstacle height h. τ_{ent} is made dimensionless by a/V_f, and h by a. $Ca = 0.0893$, $\beta = 3$ and $\zeta = 1.4$. The correlation of Bathe et al.[6] is also shown for comparison.

radius r_c. Therefore, during much of the passage the cell is entirely within the constricted segment. In our geometry, the extent of the constriction is much smaller (cf. Fig. 10), and therefore the correlation does not apply.

E. Comparison with experiment

As mentioned before, this numerical work was motivated by the experiment of Yap and Kamm,[2] and naturally the numerical results should be compared with their measurements. The experimental device includes a microchannel connecting two water-filled reservoirs that maintain a constant pressure drop during the transit of a single neutrophil (Fig. 2). By adjusting the water level, the pressure drop can be varied systematically in a series of experiments. The microchannel is rectangular in its cross section with an effective radius of 2 μm. The human neutrophils have a diameter close to 7 μm and a very large viscosity, around 2.2 poise in the adherent spread cells and even higher in passive round cells.

Yap and Kamm observed that if the pressure drop is below a threshold of 3.92 Pa (0.4 mm H$_2$O), the cell fails to enter the orifice. We observed a similar stoppage at a pressure of 3.0 Pa, and found the threshold pressure to be sensitive to the geometric parameters. For instance, the threshold is lower for the rounded corner shown in Fig. 1, and increases markedly as the entry corner gets sharper. It also increases when the reservoir-to-capillary
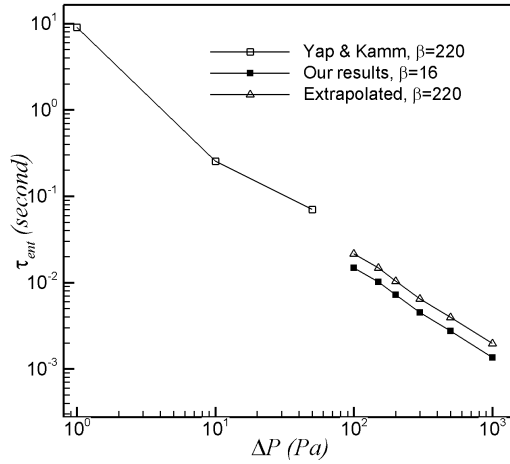
Figure 12: Comparison of the dimensional entrance time with experimental data. A pressure drop $\Delta P = 100$ Pa corresponds to $Ca = 0.0893$. In both simulations and experiments, the cell-to-capillary size ratio is $\zeta = 1.75$. The experimental viscosity ratio $\beta = 220$ for the activated cell while the simulation has $\beta = 16$. The triangles are data extrapolated from $\beta = 16$ to 220 using the 1/7 power law of Fig. 8.

contraction ratio increases. However, the resemblance between simulation and experiment may belie an important difference. In micropipette aspiration at a pressure lower than that required to suck the whole cell into the pipette, the cell seems to completely block the flow and make solid contact with the walls.[10] It is not clear whether the same happened in Yap and Kamm's experiment. In our simulations, the cell is always separated from the walls by a thin fluid layer, and the stoppage is owing to the cell's cortical tension resisting deformation.

Yap and Kamm reported entrance time data at several driving pressure drops, and these are reproduced in Fig. 12. As expected, the dimensional entrance time decreases with increasing pressure drop. We have carried out a series of simulations for comparison with the experiments. The capillary radius $a = 2$ μm matches that in the experiment. However, it is difficult to reproduce the experimental flow conditions owing to a numerical limitation. When the cell viscosity is high and/or the pressure drop is small (but still above the threshold), the cell deformation is mild and its surface is pressed against the channel walls. In the experiment, Yap and Kamm treated the PDMS walls with a copolymer surfactant solution to passivate the surface and deter cell adhesion. In the simulations,

on the other hand, there is no cell membrane. The Cahn-Hilliard energy implies neutral wettability of the cell fluid. So the cell tends to adhere to the walls with its surface at a 90° contact angle.[48,49] This problem does not arise if the cell deforms readily, say at high pressure or low cell viscosity. Thus, we have a numerical dilemma between probing low pressure and high cell viscosity. Although the difficulty can be alleviated by modifying the expression for the surface energy to increases the hydrophobicity of the wall,[56] we have not yet implemented this capability in our code. In Fig. 12, we present data for $\beta = 16$ and ΔP above the experimental range.

Despite the non-overlapping pressure ranges, the numerical data exhibit a trend that is consistent with the experimental data. Quantitatively, the numerical τ_{ent} appears lower than the experimental value, owing probably to the low β value. Since the effect of cytoplasmic viscosity has been established in subsection III.C, we have extrapolated the τ_{ent} data for $\beta = 16$ to $\beta = 220$ by using the 1/7 power law of Fig. 8. These are in better agreement with the measured values in Fig. 12; the difference is roughly 18% if extrapolated to lower ΔP.

IV. VISCOELASTIC EFFECTS

The idea of the leukocyte cytoplasm being viscoelastic comes not only from its content—numerous organelles behaving as deformable capsules and various biopolymers—but also from phenomenological observations of transient effects in micropipette aspiration.[14,21] The Maxwell model has been used to simulate cell deformation during aspiration[21] and passage through a capillary with a constriction.[6] In the latter study, Bathe *et al.* examined the transit time as dependent on the viscoelastic parameters of the model and the geometry.

We have simulated the entrance of a neutrophil when the cytoplasm is modeled as a viscoelastic Oldroyd-B fluid and the outer matrix is Newtonian. The Oldroyd-B model (cf. Eqs. 3, 4), based on a dilute suspension of elastic dumbbells in a Newtonian solvent,[52] is essentially the same as the Maxwell model except for an additional viscous stress due to the solvent. This viscous stress has two benefits: it avoids the unphysical situation of a Maxwell cell having zero viscosity at startup of deformation, and it enhances numerical stability.[41] The viscoelasticity is represented by a new dimensionless group, the Deborah number
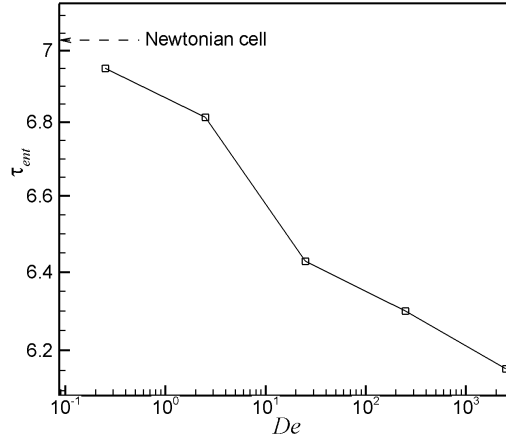
$$De = \frac{\lambda_H V_f}{a}, \tag{19}$$

21

Figure 13: The entrance time τ_{ent} decreases with the Deborah number De when the relaxation time λ_H increases. $Ca = 0.0893$, $\beta = 3$ and $\zeta = 1.4$. The arrow indicates the entrance time for the comparable Newtonian cell.

which is the relaxation time of the dumbbells λ_H scaled by the characteristic flow time $t_f = a/V_f$.

The geometry is the same as in Fig. 1, and the following parameters are used in the simulations. We fix the density ratio $\alpha = 1$ and viscosity ratio $\beta = 3$. We define β using the total viscosity $\mu_t = \mu_p + \mu_s$ of the Oldroyd-B model, with equal contribution from the polymer and the solvent: $\mu_p = \mu_s$. This β is matched with the Newtonian β when comparing with simulations in the preceding section. The radius of the undeformed cell is still $r_c = 1.4a$, and the capillary number will be given later for individual runs. Inertia is negligible. For the viscoelastic relaxation time, Bathe *et al.*[6] obtained $\lambda_H = 0.167$ s from cell indentation. Dong *et al.*[22] found a somewhat larger value of 0.25 s by fitting micropipette aspiration data. Under our flow conditions, these correspond to $De = 416$ and 624, respectively.

Figure 13 illustrates the effect of the Deborah number De on the entrance time τ_{ent} with all other parameters being fixed. This corresponds, in dimensional terms, to varying the relaxation time of the cytoplasm. The entrance time decreases monotonically when the Deborah number increases. To understand this trend, we show in Fig. 14 the flow and stress fields inside a viscoelastic cell that is roughly 2/3 through the entry. Roughly speaking, the flow field consists of three zones. The middle of the cell contains mostly rotational flow with
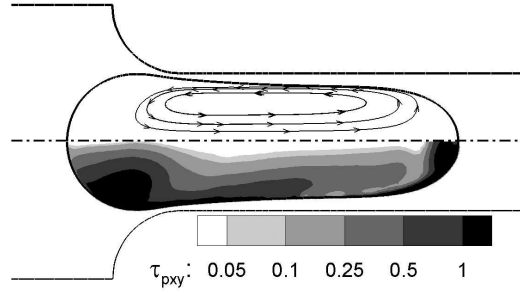
22

Figure 14: The streamline pattern (upper half) and contours of the shear stress τ_{pxy} (lower half) inside the cell during its entrance. The nominal Deborah number is $De = 25$ and the dimensionless time $t = 7.66$. The streamlines are in a reference frame fixed on the front of the cell. The shear stress is scaled by $\tau_{cell} = \mu_t u_m/a$, where u_m is the maximum horizontal velocity in the cell.

closed streamlines. The rear is practically a "dead water" zone with low deformation and stress. Finally, there is a small area in the front where the flow is extensional. Except for the front, the elastic dumbbells within the cytoplasm experience a very low level of strain rate. Note that our De is defined using the nominal shear rate V_f/a in the capillary. The actual strain rate within the cell is much smaller, and the actual De is as low as 0.15. As a result, the dumbbells largely remain in the coiled state and the stress level is low. This is reflected by the low shear stress τ_{pxy} in Fig. 14. Note that τ_{pxy} is scaled by $\tau_{cell} = \mu_t u_m/a$, u_m being the maximum horizontal velocity in the cell. The fact that $\tau_{pxy} < 1$ in most of the cell implies that the cytoplasm assumes a lower shear stress than expected for *steady shear* at the strain rate u_m/a. This is because the viscoelastic stress takes a finite time (λ_H) to develop, and attains only a fraction of τ_{cell} under the *transient strain* on the recirculating streamlines. For longer relaxation times or higher values of De, even lower levels of stress can be achieved. Therefore, the cytoplasm manifests a lower effective viscosity at a larger De. Thus, the entry time becomes shorter as the relaxation time increases for the same reason as shown in Fig. 8. This argument is also borne out by Fig. 15, which shows that with increasing De, not only the flow rate increases, but the $Q(t)$ curve develops a more prominent upswing in stage two, resembling the case of a lower cytoplasmic viscosity $\beta = 1$ in Fig. 7(a).

It is interesting to compare the above with Bathe *et al.*'s results.[6] They observed that the transit time increases with the modulus G of the Maxwell model for smaller G and levels
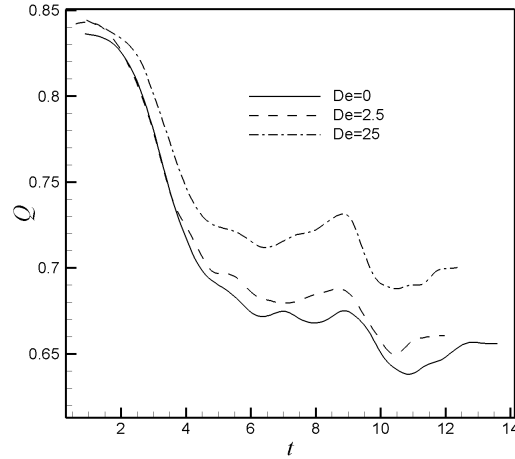
Figure 15: Effects of the Deborah number on the temporal evolution of the flow rate. $Ca = 0.0893$, $\beta = 3$ and $\zeta = 1.4$. Note that with increasing De, the $Q(t)$ curve assumes a resemblance to that of a Newtonian cell with a lower cell viscosity (cf. Fig. 7*a*).

off for large G. They interpreted the saturation as the limit of purely Newtonian rheology because the elastic spring becomes too stiff to stretch. Since the relaxation time $\lambda_H = \mu_p/G$, their increase of τ_{ent} with G corresponds to our decrease with De. Moreover, their insight on the elastic and viscous responses is entirely consistent with our analysis above. Note that Bathe *et al.* used the linear Maxwell model which would differ from our nonlinear model for large strains. This and the difference in geometry preclude a quantitative comparison. But the viscoelastic response is qualitatively the same.

The dumbbell stretching can be boosted by increasing the flow rate or ΔP while keeping the relaxation time λ_H fixed. This amounts to increasing the Deborah number De and the capillary number Ca simultaneously. Figure 16 shows that the entrance time for the viscoelastic cell increases toward that of the comparable Newtonian cell as Ca increases, and catches up with the latter approximately at $Ca = 1.01$, estimated from interpolation. For still higher ΔP, τ_{ent} exceeds that of the Newtonian cell. This is because at high flow rates, the cytoplasm experiences increasingly severe deformation and the viscoelastic stress can grow beyond that of the Newtonian fluid.[44, 52]

V. CONCLUSION

In this paper, we have examined the entrance time of a neutrophil as affected by the size and geometry of the capillary and the viscosity and viscoelasticity of the cytoplasm.
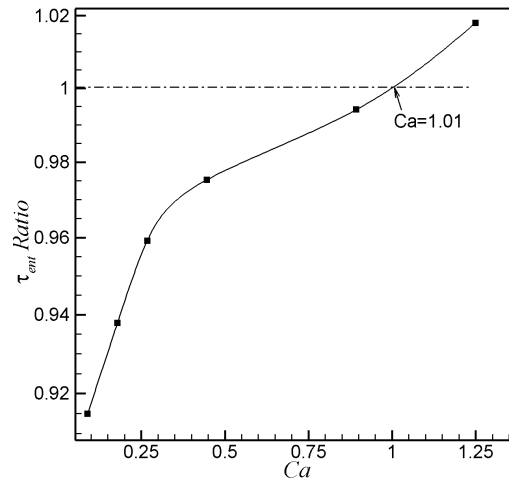
Figure 16: The ratio of entrance times between the viscoelastic cell and the Newtonian one increases with the flow rate, indicated by Ca. $\beta = 3$ and $\zeta = 1.4$. The Deborah number De increases with Ca in proportion: $De = 25$ at $Ca = 0.0893$ and $De = 250$ at $Ca = 0.893$.

The results are explained by investigating the fluid mechanics of the process. Qualitatively, the results are consistent with prior numerical and experimental data. Within the ranges of parameters covered, the results can be summarized as follows.

(a) The entrance time τ_{ent} decreases when the pressure drop over the capillary is increased, and the numerical results are in semi-quantitative agreement with the measurements of Yap and Kamm.[2]

(b) The entrance time increases sharply with decrease of the capillary diameter, and also when an obstacle inside the entry constricts the capillary.

(c) The entrance time increases with the cell viscosity according to a power-law with an index of 1/7.

(d) Viscoelasticity inside the cell tends to facilitate cell deformation and shorten τ_{ent} at moderate flow rates. With increasing flow rate, this effect is reversed when the cytoplasm develops large viscoelastic stresses.

Harking back to the sequestration of leukocytes in the lung, the longer transit time for leukocytes, as compared with erythrocytes, seems to involve two of the above mechanisms: the white cells are larger in size (b), and they have a more viscous interior than the red

cell (c). Besides, the white cell also has a highly viscous nucleus, but that is neglected in the simulations. The simulations predict the correct trend, but a more detailed comparison is hampered by simplifications in the models and the geometric setup of the simulations. In particular, we should emphasize the limitations in the physical models employed in the simulations. First, the cell membrane is represented by a fluid interface with a constant and isotropic tension. No elastic resistance to in-plane shearing and bending is incorporated. Second, the neutrophil membrane is wrinkled with roughly 100% excess area over that of a smooth sphere enclosing the same volume, whereas in our simulations, the interface in principle has unlimited extensibility. Third, the cell undergoes internal structural adaptation when it deforms and activates under mechanical load.[57] Such dynamics are ignored in our model, and indeed little work has been done on the multi-scale coupling between the cytoskeleton conformation and the mechanics of the cell as a whole. In light of the above, this work represents an initial step in an effort to simulate cell mechanics using continuum models.

References

[1] Doerschuk, C. M., N. Beyers, H. O. Coxson, B. Wiggs and J. C. Hogg. Comparison of neutrophil and capillary diameters and their relation to neutrophil sequestration in the lung. J. Appl. Physiol. 74:3040–3045, 1993.

[2] Yap, B. and R. D. Kamm. Mechanical deformation of neutrophils into narrow channels induces pseudopod projection and changes in biomechanical properties. J. Appl. Physiol. 98:1930–1939, 2005.

[3] Hogg, J. C., H. O. Coxson, M. L. Brumwell, N. Beyers, C. M. Doerschuk, W. Macnee and B. Wiggs. Erythrocyte and polymoerphonuclear cell transit-time and concentration in human pulmonary capillaries. J. Appl. Physiol. 77:1795–1800, 1994.

4 Lien, D. C., J. W. W. Wagner, R. L. Capen, C. Haslett, W. L. Hanson, S. E. Hofmeister, P. M. Henson and G. S. Worthen. Physiological neutrophil sequestration in the lung: visual evidence for localization in capillaries. J. Appl. Physiol. 62:1236–1243, 1987.

5 Huang, Y., C. M. Doerschuk and R. D. Kamm. Computational modeling of RBC and neutrophil transit through the pulmonary capillaries. J. Appl. Physiol. 90:545–564, 2001.

6 Bathe, M., A. Shirai, C. M. Doerschuk and R. D. Kamm. Neutrophil Transit Times through Pulmonary Capillaries: The Effects of Capillary Geometry and fMLP-Stimulation. Biophys. J. 83:1917–1933, 2002.

7 Wiggs, B. R., D. English, W. M. Quinlan, N. A. Doyle, J. C. Hogg and C. M. Doerschuk. Contributions of capillary pathway size and neutrophil deformability to neutrophil transit through rabbit lungs. J. Appl. Physiol. 77:463–470, 1994.

8 Doerschuk, C. M. Neutrophil rheology and transit through capillaries and sinusoids. Am. J. Respir. Crit. Care Med. 159:1693–1695, 1999.

9 Evans, E. and A. Yeung. Apparent viscosity and cortical tension of blood granulocytes determined by micropipet aspiration. Biophys. J. 56:151–160, 1989.

10 Hochmuth, R. M. Micropipette aspiration of living cells. J. Biomech. 33:15–22, 2000.

11 Fisher, T. C., R. B. Wenby and H. J. Meiselman. Pulse shape analysis of RBC micropore flow via new software for the Cell Transit Analyser (CTA). Biorheol. 29:185–201, 1992.

12 Drochon, A. Use of Cell Transit Analyser pulse height to study the deformation of erythrocytes in microchannels. Med. Eng. Phys. 27:157–165, 2005.

13 Bao, G. and S. Suresh. Cell and molecular mechanics of biological materials. Nat. Mater. 2:715–725, 2003.

14 Lim, C. T., E. H. Zhou and S. T. Quek. Mechanical models for living cells - a review. J. Biomech. 39:195–216, 2006.

15 Stamenovic, D. and D. E. Ingber. Models of cytoskeletal mechanics of adherent cells. Biomech. Model. Mechanobiol. 1:95–108, 2002.

[16] Kamm, R. D. Cellular fluid mechanics. Annu. Rev. Fluid Mech. 34:211–232, 2002.

[17] Pozrikidis, C., editor. Modeling and Simulation of Capsules and Biological Cells. Boca Raton: Chapman-Hall/CRC, 2003, 333 pp.

[18] Pozrikidis, C. Numerical simulation of cell motion in tube flow. Ann. Biomed. Eng. 33:165–178, 2005.

[19] Yeung, A. and E. Evans. Cortical shell-liquid core model for passive flow of liquid-like spherical cells into micropipets. Biophys. J. 56:139–149, 1989.

[20] Tsai, M. A., R. S. Frank and R. E. Waugh. Passive mechanical behavior of human neutrophils: power-low fluid. Biophys. J. 65:2078–2088, 1993.

[21] Dong, C., R. Skalak, K. Sung, G. Schmid-Schonbein and S. Chien. Passive deformation analysis of human leukocytes. J. Biomech. Eng. 110:27–36, 1988.

[22] Dong, C., R. Skalak and K. L. Sung. Cytoplasmic rheology of passive neutrophils. Biorheol. 28:557–567, 1991.

[23] Hochmuth, R. M., H. P. Ting-Beall, B. B. Beaty, D. Needham and R. Tran-Son-Tay. Viscosity of passive human neutrophils undergoing small deformations. Biophys. J. 64:1596–1601, 1993.

[24] Kan, H. C., H. S. Udaykumar, W. Shyy and R. Tran-Son-Tay. Hydrodynamics of a compound drop with application to leukocyte modeling. Phys. Fluids 10:760–774, 1998.

[25] Kan, H. C., W. Shyy, H. S. Udaykumar, P. Vigneron and R. Tran-Son-Tay. Effects of nucleus on leukocyte recovery. Ann. Biomed. Eng. 27:648–655, 1999.

[26] Dong, C. and R. Skalak. Leukocyte deformability: finite element modeling of large viscoelastic deformation. J. Theor. Biol. 158:173–193, 1992.

[27] Drury, J. L. and M. Dembo. Aspiration of human neutrophils: effects of shear thinning and cortical dissipation. Biophys. J. 81:3166–3177, 2001.

[28] Tran-Son-Tay, R., D. Needham, A. Yeung and R. M. Hochmuth. Time-dependent recovery of passive neutrophils after large deformation. Biophys. J. 60:856–866, 1991.

29 Tran-Son-Tay, R., H. C. Kan, H. S. Udaykumar, E. Damay and W. Shyy. Rheological modelling of leukocytes. Med. Biol. Eng. Comput. 36:246–250, 1998.

30 Pozrikidis, C. Numerical simulation of the flow-induced deformation of red blood cells. Ann. Biomed. Eng. 31:1194–1205, 2003.

31 Li, X. H. and X. Wang. The deformation of an adherent leukocyte under steady shear flow: a numerical study. J. Biomech. 37:1079–1085, 2004.

32 Khismatullin, D. B. and G. A. Truskey. Three-dimensional numerical simulation of receptor-mediated leukocyte adhesion to surfaces: Effects of cell deformability and viscoelasticity. Phys. Fluids 17:031505–21, 2005.

33 Jadhav, S., C. D. Eggleton and K. Konstantopoulos. A 3-D computational model predicts that cell deformation affects selectin-mediated leukocyte rolling. Biophys. J. 88:96–104, 2005.

34 Tran-Son-Tay, R., T. F. Kirk III, D. V. Zhelev and R. M. Hochmuth. Numerical simulation of the flow of highly viscous drops down a tapered tube. J. Biomech. Eng. 116:172–177, 1994.

35 Eggleton, C. D. and A. S. Popel. Large deformation of red blood cell ghosts in a simple shear flow. Phys. Fluids 10:1834–1845, 1998.

36 Du, Q., C. Liu and X. Wang. A phase field approach in the numerical study of the elastic bending energy for vesicle membranes. J. Comput. Phys. 198:450–468, 2004.

37 Du, Q. and L. Y. Zhu. Analysis of a mixed finite element method for a phase field bending elasticity model of vesicle membrane deformation. J. Comput. Math. 24:265–280, 2006.

38 Feng, J. and S. Weinbaum. Lubrication theory in highly compressible porous media: the mechanics of skiing, from red cells to humans. J. Fluid Mech. 422:281–317, 2000.

39 Secomb, T. W., R. Hsu and A. R. Pries. Motion of red blood cells in a capillary with an endothelial surface layer: effect of flow velocity. Am. J. Physiol. Heart Circ. Physiol. 281:H629–H636, 2001.

[40] Sethian, J. A. and P. Smereka. Level set methods for fluid interfaces. Annu. Rev. Fluid Mech. 35:341–372, 2003.

[41] Owens, R. G. and T. N. Phillips. Computational Rheology. London: Imperial College Press, 2002, 417 pp.

[42] Yue, P., J. J. Feng, C. Liu and J. Shen. A diffuse-interface method for simulating two-phase flows of complex fluids. J. Fluid Mech. 515:293–317, 2004.

[43] Feng, J. J., C. Liu, J. Shen and P. Yue. An energetic variational formulation with phase field methods for interfacial dynamics of complex fluids: advantages and challenges. In Modeling of Soft Matter, edited by M.-C. T. Calderer and E. Terentjev, New York: Springer, 2005.

[44] Yue, P., J. J. Feng, C. Liu and J. Shen. Diffuse-Interface Simulations of Drop Coalescence and Retraction in Viscoelastic Fluids. J. Non-Newtonian Fluid Mech. 129:163–176, 2005.

[45] Yue, P., J. J. Feng, C. Liu and J. Shen. Interfacial force and Marangoni flow on a nematic drop retracting in an isotropic fluid. J. Colloid Interface Sci. 290:281–288, 2005.

[46] Yue, P., J. J. Feng, C. Liu and J. Shen. Viscoelastic effects on drop deformation in steady shear. J. Fluid Mech. 540:427–437, 2005.

[47] Yue, P., J. J. Feng, C. Liu and J. Shen. Transient Drop Deformation upon Startup of Shear in Viscoelastic Fluids. Phys. Fluids 17:123101, 2005.

[48] Yue, P., C. Zhou, J. J. Feng, C. F. Ollivier-Gooch and H. H. Hu. Phase-Field Simulations of Interfacial Dynamics in Viscoelastic Fluids Using Finite Elements with Adaptive Meshing. J. Comput. Phys. 219:47–67, 2006.

[49] Zhou, C., P. Yue and J. J. Feng. Formation of simple and compound drops in microfluidics devices. Phys. Fluids 18:092105, 2006.

[50] Yue, P., C. Zhou and J. J. Feng. A computational study of the coalescence between a drop and an interface in Newtonian and viscoelastic fluids. Phys. Fluids 18:102102, 2006.

[51] Lowengrub, J. and L. Truskinovsky. Quasi-incompressible Cahn-Hilliard fluids and topological transitions. Proc. Roy. Soc. Lond. A 454:2617–2654, 1998.

[52] Bird, R. B., R. C. Armstrong and O. Hassager. Dynamics of Polymeric Liquids, Vol. 1. Fluid Mechanics. New York: Wiley, 1987, 649 pp.

[53] Freitag, L. A. and C. F. Ollivier-Gooch. Tetrahedral Mesh Improvement Using Swapping and Smoothing. Int. J. Numer. Methods Eng. 40:3979–4002, 1997.

[54] Yoeli, M. and B. J. Hargreaves. Brain capillary blockage produced by a virulent strain of rodent malaria. Science 184:572–573, 1974.

[55] Shelby, J. P., J. White, K. Ganesan, P. K. Rathod and D. T. Chiu. A microfluidic model for single-cell capillary obstruction by plasmodium falciparum-infected erythrocytes. PNAS 100:14618–14622, 2003.

[56] Jacqmin, D. Contact-line dynamics of a diffuse fluid interface. J. Fluid Mech. 402:57–88, 2000.

[57] Yap, B. and R. D. Kamm. Cytoskeletal remodeling and cellular activation during deformation of neutrophils into narrow channels. J. Appl. Physiol. 99:2323–2330, 2005.